DYNAMICS MODELING AND PERFORMANCE EVALUATION OF AN AUTONOMOUS UNDERWATER VEHICLE

Jason Evans, Meyer Nahon
Dept. of Mechanical Engineering
McGill University
Montreal, Quebec, Canada, H3A 2K6
Jason.Evans@mcgill.ca Meyer.Nahon@mcgill.ca

Abstract

This paper describes a dynamics model of an autonomous underwater vehicle (AUV). External forces acting on the vehicle, such as hull and control plane hydrodynamic forces, are determined for the full 360˚ angle of attack range. An accurate through-body thruster model is also incorporated into the simulation. The model is used to simulate two configurations of the C-SCOUT AUV. We use the simulation as a predictive design tool to evaluate and compare the performance of the two configurations before they have been fully developed. Two oceanographic sampling missions are devised to help determine the relative benefits of each configuration.

1. Introduction

A. *Autonomous Underwater Vehicles*

In recent years, autonomous underwater vehicles (AUVs) have had an increasingly pervasive role in underwater research and exploration. These vehicles generally have a streamlined, torpedo-shaped body, and are intended for long-distance missions where their low drag enables high speeds and coverage of a large distance. Hydrodynamic fins are used to direct the vehicle and rely on forward motion to generate the forces required to change orientation. Some AUVs use a combination of hydrodynamic fins and through-body thrusters for control of the vehicle. Through-body thrusters enable orientation control at low speeds, while the fins provide control at higher speeds. Examples of these AUVs include the NPS ARIES [1], NPS PHOENIX, Proteus [2], OTTER [3], CETUS, REDERMOR [4], and C-SCOUT [5].

B. *The C-SCOUT AUV*

C-SCOUT (Canadian Self-Contained Off-the-shelf Underwater Testbed) is an AUV currently being developed at Memorial University of Newfoundland (MUN) in St. John's, Newfoundland [5]. It is a joint project between the Institute for Marine Dynamics (IMD) and MUN's Ocean Engineering Research Center. The research program is aimed at assessing the impact of discharges from offshore oil platforms and gas operations through the development of AUVs for environmental missions [6].

C-SCOUT is designed and built with modularity in mind [5]. By incorporating multiple modules that can be interchanged, a highly configurable vehicle is obtained. These modules can contain electronics, fin actuators, sensors, ballast, through-body thrusters, and body contours. In all its configurations C-SCOUT is a streamlined AUV, designed for speed and the ability to cover large distances.

The two configurations that are currently being evaluated are the Baseline Configuration (BC) and the Fully-Actuated Configuration (FAC) (see *Figure 1*). Each configuration adds modules to a basic hull, thereby lengthening the vehicle. The basic hull has an ellipsoidal nose, a cylindrical mid-section, and a cubic spline tail section. Contained in the basic hull are the components required for AUV operations, such as obstacle avoidance sonar, a computer system, a navigation and orientation system, an energy storage system, payload such as cameras or oceanographic sensors, and ballast. The vehicle always maintains neutral buoyancy and therefore relies on hydrodynamic forces generated by the control planes or through-body thrusters for depth control. Except for the pressure vessel, which contains the electronics of the vehicle, the hull is free-flooding, making sealing unnecessary. Conversion from one configuration to another is nominally a simple matter of removing bolts and inserting or removing a module. The rear thruster is common to both configurations.

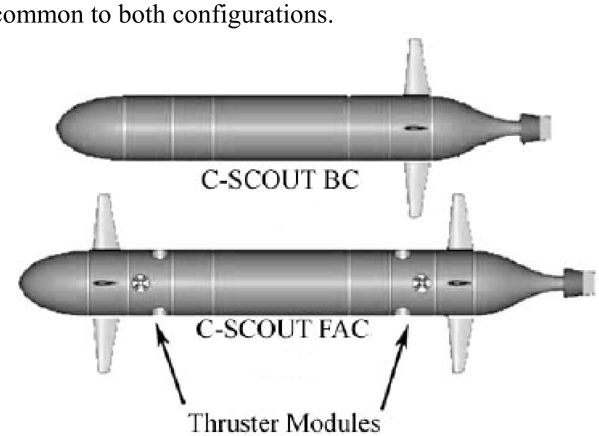

Figure 1 – C-SCOUT Baseline and Fully Actuated Configurations (Top View)

The Baseline Configuration adds a control plane module to the basic hull at the rear of the vehicle. The control plane module consists of two vertical control planes, two horizontal control planes, and an independently controlled actuator for each plane.

Currently, this configuration has been constructed and is undergoing testing at IMD and Memorial University. Thus far, testing of C-SCOUT has been limited to remote control in the Ocean Engineering Basin at IMD.

The Fully Actuated Configuration adds to the basic hull two control plane modules, each containing two vertical control planes, two horizontal control planes, and actuators. One module is located at the rear of the vehicle and one is located at the front. Also included in this configuration are two through-body thruster modules, each containing two horizontal thrusters and one vertical thruster. One of these modules is located in front of the rear control plane module, and the other behind the front control plane module.

The through-body thrusters are intended to improve the maneuverability of the vehicle at low speeds and to give the vehicle the ability to hover in a cross-flow.

C. AUV Simulations

Development and testing of an AUV is a lengthy and costly undertaking. Not only does one risk the loss of the vehicle due to various computer errors, but also the cost of a support crew, equipment, and facilities can be prohibitively expensive. Thus, computer modeling of the vehicle is important to the AUV designer. A model of the vehicle can help evaluate the effects of body profile, configuration, controllers, and environmental factors without risking the loss of the actual vehicle. One of the major challenges in creating such a computer model is that the vehicle dynamics must be accurately represented; otherwise there is a risk of designing a vehicle and controllers based on erroneous information.

To fully describe the motion of an AUV, a 6 degree-of-freedom simulation is required. The dynamics of the vehicle are represented by six second-order differential equations, one for each degree of freedom of the vehicle. Once the external forces on the vehicle are determined, the accelerations in each degree of freedom can be calculated by solving the motion equations.

Hydrodynamic derivatives are commonly used to characterize the external forces on the vehicle. These are coefficients that quantify the forces on the vehicle as a function of its attitude and motion. The use of hydrodynamic derivatives in a simulation can provide very realistic results, as long as the derivatives are accurately evaluated. Hydrodynamic derivatives can be determined either by test-based or predictive methods. The major disadvantage of test-based methods is the need for a vehicle and the tests themselves, which can be prohibitively expensive and time consuming. Predictive methods, such as the approach presented by DATCOM [7], can yield reasonable results if the geometry of the vehicle is not too complex. Researchers who have used hydrodynamic derivatives in their AUV simulations include Hopkin and den Hertog [8], Encarnaca and Pascoal [9], Cristi et. al. [10], and Humphreys and Smith [11].

Another approach used to calculate the external forces on a vehicle is the component buildup method. In this method, hydrodynamic forces are derived from empirical relations that only require specification of the vehicle geometry. Each component of the vehicle, such as the hull, control surfaces, and thrusters, is modeled separately using simple hydrodynamic relations. The forces and moments from each of these components are summed together to provide the total forces and moments acting on the hull. Use of this method enables the model to retain the vehicle's nonlinear behavior. Researchers who have used the component buildup method in their AUV simulations include Nahon [12], Perrault [13], and Prestero [14].

A major drawback to the simulations presented by the researchers who have implemented the component buildup method is a limitation to small angles of attack on the hull and control planes. At low velocities, or in the case of a crosscurrent, large angles of attack can occur. For example, a vehicle performing stationkeeping in a crosscurrent can experience an angle of attack of 90˚ on the hull and vertical control planes. Thus we desire a simulation that can handle the full 360˚ angle of attack range. Also in order to model the C-SCOUT Fully Actuated Configuration, we need to include an accurate model of through-body thrusters.

This paper describes an AUV dynamics model and simulation. The model relies on the component buildup method to evaluate forces on the vehicle and has the capability to handle the full 360˚ angle of attack range on the hull, control planes, and through-body thrusters. Performance capabilities such as predicted turning diameters and vehicle stability of the C-SCOUT Baseline and Fully-Actuated Configurations are compared. An evaluation of the ability of each configuration to complete a mission is then determined based on a simple set of control laws and tactics.

2. Vehicle Model

A. Motion Equations

Nahon's [12] vehicle dynamics model is based on a set of dynamic equations that govern the vehicle's translational and rotational motion in 3-D space. The vehicle is considered to have 6 degrees of freedom: surge, sway, heave, roll, pitch, and yaw (see *Figure 2)*

The translational motions follow Newton's law, written as:

$$\mathbf{F} = m\mathbf{a}_{\mathrm{cm}} \tag{1}$$

where $\mathbf{F}$ is the net external force applied to the vehicle, m is the mass of the vehicle, and $\mathbf{a}_{\mathrm{cm}}$ is the acceleration of its mass center with respect to an inertial frame. The rotational motions follow Euler's equations:

$$\mathbf{M}_{\mathrm{cm}} = \mathbf{I}_{\mathrm{cm}}\dot{\boldsymbol{\omega}} + \boldsymbol{\omega} \times \mathbf{I}_{\mathrm{cm}}\boldsymbol{\omega} \tag{2}$$

where $\mathbf{M}_{cm}$ is the net external moment acting on the vehicle at the center of mass, $\mathbf{I}_{cm}$ is the inertia tensor about the vehicle's mass center, and $\boldsymbol{\omega}$ is the vehicle's angular velocity vector.

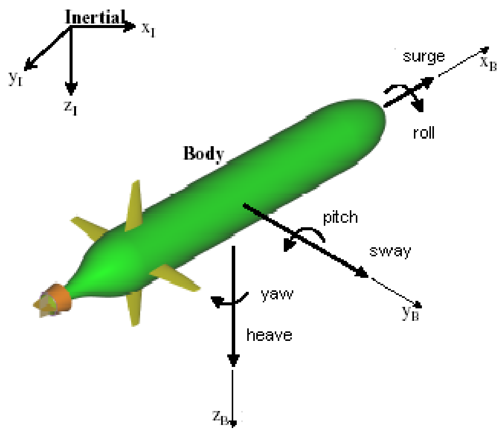

Figure 2– Vehicle Motions

The external forces and moments on the vehicle are due to the following effects:

- Gravitational
- Buoyancy
- Propulsive
- Control
- Hydrodynamic

The motion equations given by (1) and (2) can also be written in the form [12]:

$$\ddot{\mathbf{q}} = \mathbf{M}^{-1}\left[\boldsymbol{\tau} - \mathbf{h}\left(\mathbf{x}, \dot{\mathbf{q}}\right)\right] \tag{3}$$

where $\mathbf{M} \in \mathbf{R}^{6x6}$ is the inertia matrix including added mass, $\mathbf{h}\left(\mathbf{x}, \dot{\mathbf{q}}\right) \in \mathbf{R}^6$ is a vector that includes centrifugal, Coriolis, gravitational, buoyancy, and hydrodynamic forces, and $\boldsymbol{\tau} \in \mathbf{R}^6$ is a vector of control forces. $\mathbf{x}$ is the position state vector in the inertial frame, $\dot{\mathbf{q}}$ is the velocity state vector in the body-fixed frame, and $\ddot{\mathbf{q}}$ is the acceleration vector in the body-fixed frame:

$$\mathbf{x} = \begin{bmatrix} X & Y & Z & \phi & \theta & \psi \end{bmatrix}^{\mathrm{T}}$$
$$\dot{\mathbf{q}} = \begin{bmatrix} u & v & w & p & q & r \end{bmatrix}^{\mathrm{T}}$$

where X, Y, and Z are the inertial coordinates of the center of mass of the vehicle, ϕ, θ, and ψ are the three Euler angles (roll, pitch, yaw) that specify the vehicle's orientation in space, u, v, and w are the translational velocities in the body-fixed frame, and p, q, and r are the rotational velocities in the body-fixed frame.

Once we have determined the forces on the vehicle, we can calculate the accelerations in the body-fixed frame, shown in (3). We can then integrate (3) to obtain the vehicle's velocities and position, which can be transformed back into the inertial frame. More detail on this procedure is given in [12].

B. Hull Forces

The hull force calculation described in Nahon's [12] simulation is not suitable for large angles of attack, and so must be improved for the present purpose. We begin by reviewing research on hull forces for streamlined bodies in order to choose a suitable formulation.

Various researchers have attempted to estimate the hull forces for a streamlined body of revolution at angles of attack. Munk [15] proposed the idea that the hull force on airships can be estimated by a potential flow analysis of the flow around a streamlined body. This analysis is equally valid for an underwater vehicle. Allen and Perkins [16] built on this idea by performing a viscous cross-flow analysis. This generated a viscous-flow term, which can be added to Munk's potential term. Hopkins [17] followed a similar analysis to Allen and Perkins, but changed the limits of integration on the hull to have the potential term acting only along the forward portion of the hull, and the viscous term acting along the aft of the hull.

Unfortunately these analyses by Munk, Allen and Perkins, and Hopkins are accurate only for low angles of attack (up to about 12˚) [7]. We desire a formulation that is valid for the full 360˚ angle of attack range, as it is likely that an AUV will encounter this range while traveling slowly or in the presence of a cross-flow. Jorgensen [18] presents a formulation that is valid for the full 360˚ angle of attack range. We implement this method in our simulation, with one variation: Jorgensen neglects the added mass factor (k_2-k_1), which was initially presented by Munk [15]. This is valid for high fineness ratio (length/diameter) hulls, for which (k_2-k_1) is about equal to 1. As we will not necessarily have a high fineness ratio hull in our simulation, we include the added mass factor in our formulation. The hull normal, axial, and pitching moment coefficients therefore become:

For $0^\circ \le \alpha \le 90^\circ$:

$$C_A = C_{DF(\alpha=0^\circ)} \cos^2 \alpha'$$
$$C_M = \left(k_2 - k_1\right)\left[\frac{V_B - S_b\left(l - x_m\right)}{AX}\right]\sin 2\alpha' \cos\frac{\alpha'}{2} + \eta C_{Dc}\frac{A_p}{A}\left(\frac{x_m - x_p}{X}\right)\sin^2 \alpha'$$

For $90^\circ \le \alpha \le 180^\circ$ (4)

$$C_A = C_{DF(\alpha=180^\circ)} \cos^2 \alpha'$$
$$C_M = -\left(k_2 - k_1\right)\left[\frac{V_B - S_b x_m}{AX}\right]\sin 2\alpha' \cos\frac{\alpha'}{2} + \eta C_{Dc}\frac{A_p}{A}\left(\frac{x_m - x_p}{X}\right)\sin^2 \alpha'$$

For $0^\circ \le \alpha \le 180^\circ$:

$$C_N = \left(k_2 - k_1\right)\frac{S_b}{A}\sin 2\alpha' \cos\frac{\alpha'}{2} + \eta C_{Dc}\frac{A_p}{A}\sin^2 \alpha'$$

where

$\alpha' = \alpha$ for $0^\circ \le \alpha \le 90^\circ$

$\alpha' = 180^\circ - \alpha$ for $90^\circ \le \alpha \le 180^\circ$

and C_A, C_N, and C_M are the axial, normal, and pitching moment coefficients, respectively (see *Figure 3*), $C_{DF(\alpha=0^\circ)}$ and $C_{DF(\alpha=180^\circ)}$ are the form drag coefficients of the hull at an angle of attack of 0˚ and 180˚, respectively, V_B is the hull volume, S_b is the cross-sectional base area of the hull (we assume that the hull has a blunt base, as Jorgensen's equations were intended for, and S_b is equal to the maximum cross-sectional area of the hull), l is the hull length, x_m is the distance from the nose to the pitching moment center, which we will choose as the center of mass, A and X are the reference area and length (we will use the wetted area and the length of the hull, respectively), η is the cross-flow drag proportionality factor (ratio of the cross-flow drag coefficient for a finite length cylinder to that of an infinite length cylinder, see *Figure 4*), C_{Dc} is the cross-flow drag coefficient of a circular cylinder (see *Figure 5*), A_p is the planform area of the hull, and x_p is the distance from the nose to the centroid of the planform area of the hull. α is the hull angle of attack (see *Figure 6*), defined as:

$$\alpha = \tan^{-1}\left(\frac{\sqrt{{v_{CE}}^2 + {w_{CE}}^2}}{u_{CE}}\right) \tag{5}$$

Note that based on (5), α will lie between 0˚ and 180˚. The 180˚ to 360˚ range is accounted for by the rotation angle, Φ, specifying the velocity vector location in the body-fixed *Y-Z* plane (see *Figure 6*).

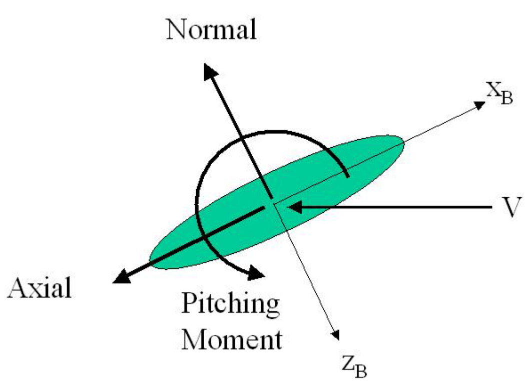

Figure 3 – Illustration of Normal and Axial Forces on Hull

The subscript *CE* designates the center of pressure of the hull, which we term the center of effort [13]. Due to the symmetrical characteristics of most AUVs, the center of effort is located on the longitudinal axis, at a longitudinal location that moves aft with increasing angle of attack [18]. It generally lies ahead of the center of mass and can even extend ahead of the nose at low angles of attack. The velocity components at the center of effort can be calculated from those at the center of mass as follows:

$$\begin{bmatrix} u_{CE} \\ v_{CE} \\ w_{CE} \end{bmatrix} = \begin{bmatrix} u \\ v \\ w \end{bmatrix} + \begin{bmatrix} p \\ q \\ r \end{bmatrix} \times \begin{bmatrix} x_{CE} \\ y_{CE} \\ z_{CE} \end{bmatrix} \tag{6}$$

where y_{CE} and z_{CE} are equal to the distance from the center of mass to the longitudinal axis of the hull along the y and z body-fixed axes, and the longitudinal position of the center of effort, x_{CE}, is calculated using:

$$x_{CE} = \frac{XC_M}{C_N} \tag{7}$$

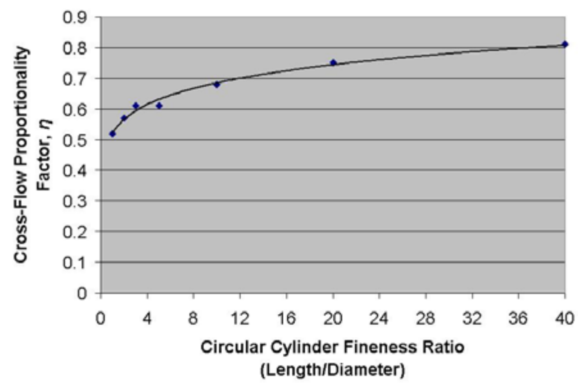

Figure 4 – Cross-Flow Drag Proportionality Factor [18]

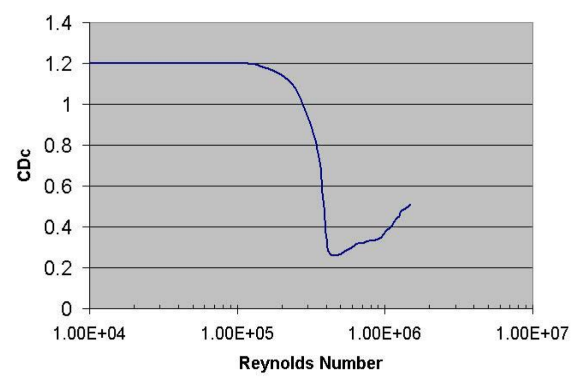

Figure 5 – Cross-Flow Drag Coefficient [18]

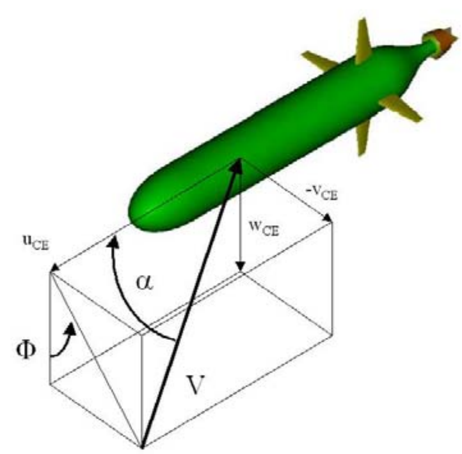

Figure 6 – Illustration of Hull Angles

The forces on the hull expressed in the body-fixed frame are computed as follows:

$$\begin{bmatrix} X_{Hull} \\ Y_{Hull} \\ Z_{Hull} \end{bmatrix} = \frac{1}{2}\rho A V_{CE}^{2} \begin{bmatrix} -1 & 0 & 0 \\ 0 & \sin\Phi & 0 \\ 0 & -\cos\Phi & 0 \end{bmatrix} \begin{bmatrix} C_A \\ C_N \\ 0 \end{bmatrix} \quad (8)$$

where ρ is the fluid density, V_{CE} is the total velocity at the center of effort, and Φ is the rotation angle (see *Figure 6*), defined as:

$$\Phi = \tan^{-1}\left(\frac{-v_{CE}}{w_{CE}}\right) \quad (9)$$

The point of application of the forces is at the center of effort of the hull. Therefore the moments about the center of mass due to the hull forces are calculated as the applied hull force multiplied by $\mathbf{r}_{\mathrm{CE}}$, the moment arm from the center of mass to the center of effort:

$$\mathbf{M}_{\mathrm{Hull}} = \mathbf{r}_{\mathrm{CE}} \times \mathbf{F}_{\mathrm{Hull}} \quad (10)$$

Drag resistance testing has been performed on the basic hull of C-SCOUT in the tow tank at Memorial University for forward velocities up to 2.5 m/s [19]. From these experimental results we can estimate the drag coefficient on the basic hull for zero angle of attack without the control planes. A drag coefficient of $C_{DF(\alpha=0^{\circ})}$ = 0.0077, based on the wetted area of the hull, achieves a good fit to the empirical data (see *Figure 7*). We will assume that the drag coefficient is the same for the Baseline and Fully Actuated Configurations.

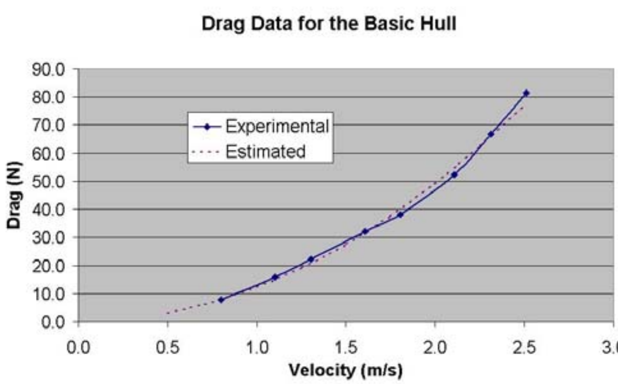

Figure 7 – C-SCOUT Basic Hull Drag Data

C. Control Plane Forces

Hydrodynamic control planes provide orientation control for the vehicle while it is in motion. Traditionally the forces are decomposed into lift and drag forces, perpendicular and parallel to the incident fluid flow, respectively (see *Figure 8)*.

Lift and Drag coefficients for 2-D sections are readily available for a wide variety of wing sections at angles of attack up to the point of stall (e.g. [20]). However, we desire a simulation that is capable of the full 360º range of angles. Few researchers have looked at such a wide range of angles, due to the limited usefulness of angles of attack beyond stall in aircraft operations. Two researchers that have looked at airfoil behavior at large angles of attack are Riegels [21] and Critzos et. al. [22] (see *Figures 9* and *10*).

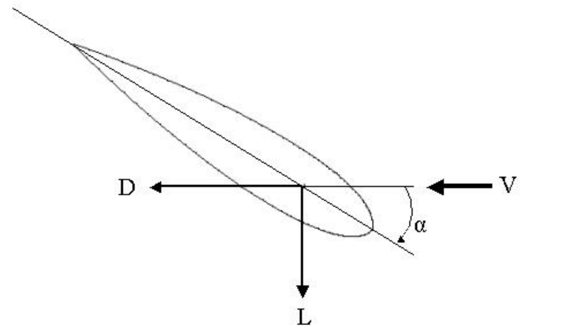

Figure 8 – Illustration of Lift and Drag on an Airfoil

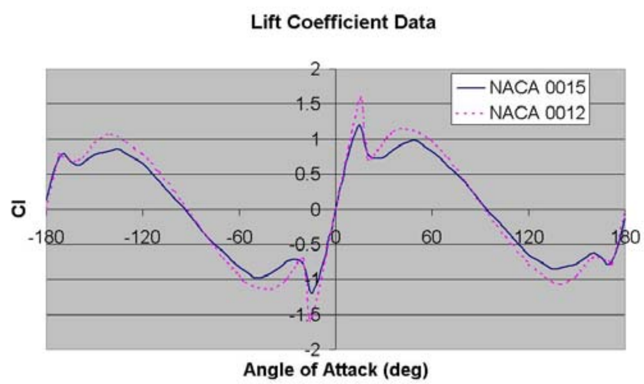

Figure 9 – Lift Coefficient Data Over 360˚ Range for NACA 0012 [21] and NACA 0015 [22] Wing Sections

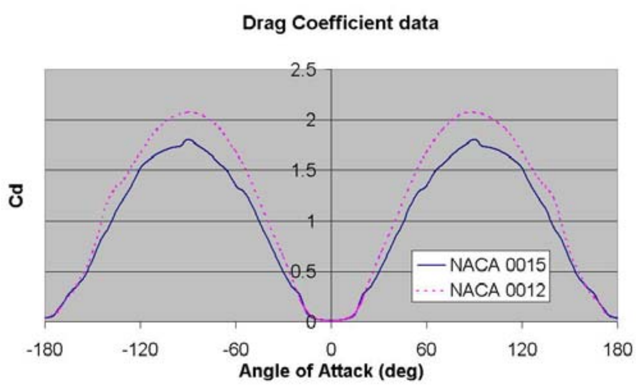

Figure 10 – Drag Coefficient Data Over 360˚ Range for NACA 0012 [21] and NACA 0015 [22] Wing Sections

Modifying the 2-D wind section lift and drag coefficients to apply to 3-D wing can be accomplished with methods such as those presented by McCormick [23]:

$$C_L = \frac{a_e C_l}{a_e + 2\left(\frac{a_e + 4}{a_e + 2}\right)} \quad (11)$$

$$C_D = f_{CD} C_d \quad (12)$$

where a_e is the effective aspect ratio of the plane, defined below, C_l and C_d are the 2-D section lift and drag coefficients, respectively, and f_{CD} is a scale factor from McCormick [23], *Figure 4.11*. Note that (11) is intended for the linear angle of attack range before stall, but is assumed valid here for the nonlinear range as well. The effective aspect ratio of the plane is defined as:

$$a_e = \frac{{b_{CP}}^2}{A_{CP}} \tag{13}$$

where b_{CP} is the span (twice the distance from the root to the tip of the control plane) and A_{CP} is the planform area of a set of control planes, without the area included inside the hull. We do not include the area inside the hull (inclusion of this area is commonly performed in aircraft analysis) due to the large hull size compared to the control plane size. Including this area inside the hull would increase the control plane area by almost 2-fold.

The lift and drag coefficients for the horizontal planes are a function of the angle of attack and the plane deflection. The lift and drag coefficients for the vertical planes are a function of the angle of sideslip and the plane deflection. The angle of attack and sideslip angle for the horizontal control planes are computed as:

$$\left(\alpha_{CP}\right)_{hor} = \tan^{-1}\left(\frac{w_{CP}}{u_{CP}}\right) \tag{14}$$

$$\left(\beta_{CP}\right)_{hor} = \tan^{-1}\left(\frac{v_{CP}}{\sqrt{{u_{CP}}^2 + {w_{CP}}^2}}\right) \tag{15}$$

while for the vertical control planes, they are computed as:

$$\left(\alpha_{CP}\right)_{ver} = \tan^{-1}\left(\frac{w_{CP}}{\sqrt{{u_{CP}}^2 + {v_{CP}}^2}}\right) \tag{16}$$

$$\left(\beta_{CP}\right)_{ver} = \tan^{-1}\left(\frac{v_{CP}}{u_{CP}}\right) \tag{17}$$

Estimation of lift and drag forces on the planes in 3-D fluid flow is another issue to be considered. Lift and drag coefficients are typically provided as a function of angle of attack only. Thus we must make an assumption when the plane experiences sideslip. To account for this, we calculate the control plane's lift and drag forces, neglecting the cross-plane velocity component. Lift and drag on the horizontal control planes are calculated as follows:

$$\left(L_{CP}\right)_{hor} = \frac{1}{2}\rho A C_L \left[V_{CP}\cos\left(\beta_{CP}\right)_{hor}\right]^2 \tag{18}$$

$$\left(D_{CP}\right)_{hor} = \frac{1}{2}\rho A C_D \left[V_{CP}\cos\left(\beta_{CP}\right)_{hor}\right]^2 \tag{19}$$

while on the vertical control planes, they are calculated as follows:

$$\left(L_{CP}\right)_{ver} = \frac{1}{2}\rho A C_L \left[V_{CP}\cos\left(\alpha_{CP}\right)_{ver}\right]^2 \tag{20}$$

$$\left(D_{CP}\right)_{ver} = \frac{1}{2}\rho A C_D \left[V_{CP}\cos\left(\alpha_{CP}\right)_{ver}\right]^2 \tag{21}$$

The control plane forces in the body frame, acting at the center of pressure of the control planes (defined below), are computed as:

$$\begin{bmatrix} X_{CP} \\ Y_{CP} \\ Z_{CP} \end{bmatrix}_{hor} = \begin{bmatrix} -\cos\left(\alpha_{CP}\right)_{hor} & 0 & \sin\left(\alpha_{CP}\right)_{hor} \\ 0 & 1 & 0 \\ -\sin\left(\alpha_{CP}\right)_{hor} & 0 & -\cos\left(\alpha_{CP}\right)_{hor} \end{bmatrix} \begin{bmatrix} D_{CP} \\ 0 \\ L_{CP} \end{bmatrix}_{hor} \tag{22}$$

$$\begin{bmatrix} X_{CP} \\ Y_{CP} \\ Z_{CP} \end{bmatrix}_{ver} = \begin{bmatrix} -\cos\left(\beta_{CP}\right)_{ver} & \sin\left(\beta_{CP}\right)_{ver} & 0 \\ -\sin\left(\beta_{CP}\right)_{ver} & -\cos\left(\beta_{CP}\right)_{ver} & 0 \\ 0 & 0 & 1 \end{bmatrix} \begin{bmatrix} D_{CP} \\ L_{CP} \\ 0 \end{bmatrix}_{ver} \tag{23}$$

External moments on the vehicle due to the forces on the control planes are expressed in the body frame as:

$$\mathbf{M}_{\mathrm{CP}} = \mathbf{r}_{\mathrm{CP}} \times \mathbf{F}_{\mathrm{CP}} \tag{24}$$

where $\mathbf{r}_{\mathrm{CP}}$ is a vector from the center of mass of the vehicle to the center of pressure of the control plane. The center of pressure of the control plane is assumed to be at the quarter-chord point of the section at 42% of the halfspan out from the root chord [13].

D. *Through-Body Thrusters*

C-SCOUT uses through-body thrusters in its Fully Actuated Configuration, and we therefore require a method of modeling these thrusters in the vehicle simulation. Saunders and Nahon [24] have studied the effects of forward speed and vehicle orientation on through-body thruster performance. They created a dynamics model of a through-body thruster incorporating yaw angle and forward velocity, specific to C-SCOUT. Here, we briefly discuss that model and how it is incorporated into our simulation. The through-body thruster model is described by a first-order differential equation:

$$F_a = \rho A_D l_D \gamma \dot{U}_a + a + b\omega_p\left|\omega_p\right| \tag{25}$$

where F_a is the output thrust, A_D and l_D are the duct area and length, respectively, γ is an empirically determined added mass coefficient, $\dot{U}_a$ is the time derivative of the fluid velocity at the propeller, and a and b are vehicle-specific, experimentally determined coefficients, that vary with yaw angle and forward velocity of the vehicle. The first term in (25) represents the transient effects of the thruster, and the second and third terms represent the steady-state effects.

Saunders and Nahon obtained values for a and b for a forward through-body thruster mounted horizontally on C-

SCOUT for sideslip angles from -90˚ to 90˚ and forward vehicle velocities from 0 to 4 m/s. In our simulation of C-SCOUT, we assume that those values for a and b are independent of thruster position and orientation on the vehicle. During the simulation, a and b are selected from look-up tables based on the sideslip angle and forward speed. Velocity components at the center of the through-body thruster are computed as:

$$\begin{bmatrix} u_{TT} \\ v_{TT} \\ w_{TT} \end{bmatrix} = \begin{bmatrix} u \\ v \\ w \end{bmatrix} + \begin{bmatrix} p \\ q \\ r \end{bmatrix} \times \begin{bmatrix} x_{TT} \\ y_{TT} \\ z_{TT} \end{bmatrix} \tag{27}$$

where x_{TT}, y_{TT}, and z_{TT} are the locations of the center of the through-body thruster with respect to the center of mass in the body-fixed frame. In the calculation of the total forward velocity to be used in the look-up tables of a and b, we obtain the projection of the velocity vector onto the plane defined by the axis of the though-body thruster and the longitudinal axis of the vehicle:

$$\left(V_{TT}\right)_{hor} = \sqrt{u_{TT}{}^2 + v_{TT}{}^2} \tag{28}$$

$$\left(V_{TT}\right)_{ver} = \sqrt{u_{TT}{}^2 + w_{TT}{}^2} \tag{29}$$

where the subscripts, *hor* and *ver* describe a horizontal or vertical thruster orientation on the vehicle, respectively. The sideslip angle at the through-body thrusters is then computed as follows:

$$\left(\beta_{TT}\right)_{hor} = \tan^{-1}\left(\frac{v_{TT}}{u_{TT}}\right) \tag{30}$$

$$\left(\beta_{TT}\right)_{ver} = \tan^{-1}\left(\frac{w_{TT}}{u_{TT}}\right) \tag{31}$$

The force exerted by each through-body thruster on the hull, $\mathbf{F}_{\mathrm{TT}}$, acting along the axis of the thruster, is calculated using (25). $\mathbf{F}_{\mathrm{TT}}$ will have only one non-zero component if the thruster is oriented parallel to one of the vehicle axes. The corresponding moment is then:

$$\mathbf{M}_{\mathrm{TT}} = \mathbf{r}_{\mathrm{TT}} \times \mathbf{F}_{\mathrm{TT}} \tag{32}$$

where $\mathbf{r}_{\mathrm{TT}} = \begin{bmatrix} x_{TT} & y_{TT} & z_{TT} \end{bmatrix}^{\mathrm{T}}$.

E. Rear Thruster

The rear thruster is simply modeled as a force exerted along the longitudinal axis of the vehicle. At equilibrium, this thrust will equal the drag of the vehicle, and no acceleration will occur. Once the vehicle is in motion, the thrust is inversely proportional to the forward velocity of the vehicle:

$$T = \frac{T_0 V_0}{u} \tag{33}$$

where T is the thrust and T_0 is equal to the drag of the vehicle at its initial equilibrium velocity, V_0.

3. Model Validation Using ARCS Vehicle

One of the valuable aspects of an AUV simulation is its ability to evaluate a vehicle's performance before it has been constructed. We wish to know how the performance of the Baseline Configuration will compare to that of the Fully-Actuated Configuration. Our vehicle simulation is coded in Simulink®. Before using it to evaluate C-SCOUT's performance, we wish to know if it is accurate. However, validation data is currently available for C-SCOUT, though it is expected to become available for the Baseline Configuration in the near future. For validation, we will model the ARCS vehicle, for which extensive experimental data is available.

A. The ARCS Vehicle

ARCS [25] is an AUV developed by International Submarine Engineering (ISE) and used as a test bed for evaluating AUV technologies (see *Figure 11*). The vehicle is described in more detail in [8] and [12].

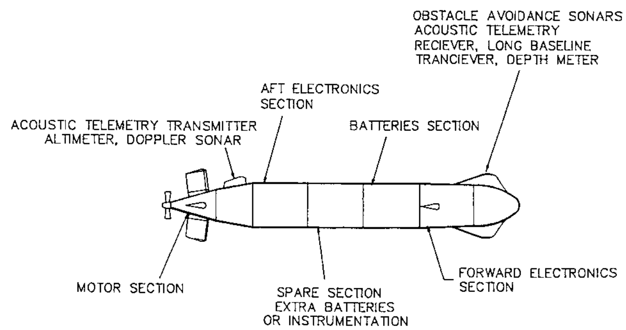

Figure 11 – Side View of the ISE ARCS Vehicle

In the case of ARCS, some aspects of the simulation are performed differently than mentioned in Section 2. More specifically, the hull drag at zero angle of attack is estimated using a method proposed by Humphreys and Smith [11], while the control plane lift curve slopes are determined based on experimental data found in [8]. These details are discussed more extensively in [12].

B. Model Validation

Using the ARCS vehicle model in our simulation, we can compare simulated results to field test data obtained by Hopkin and den Hertog [8]. Hopkin and den Hertog list turning diameters for three vehicle velocity and rudder deflection combinations of the ARCS. Although this is not a thorough validation, it does give us an indication of the accuracy of our simulation. *Table 1* compares the results of our simulation and the field test data.

The simulated turning diameters of the ARCS closely match the measured field data. Discrepancies between these results are likely due to assumptions made in modeling the control planes and bulges of the ARCS vehicle.

Turning Diameters			
	25˚ rudder deflection at 1.5 m/s	25˚ rudder deflection at 2.5 m/s	15˚ rudder deflection at 2.5 m/s
Measured Field Data [8]	32.9 m	34.8 m	51.8 m
Simulated Motion	32.5 m	33.1 m	58.8 m

Table 1 – Measured and Predicted Turning Diameters for the ARCS Vehicle

4. C-SCOUT Simulation Results

We can now compare the performance of C-SCOUT's Baseline and Fully Actuated Configurations by examining the stability, turning diameter, and turning response (defined as the time it takes for the vehicle to turn 180˚) for each configuration at various vehicle speeds and control inputs. For the Baseline Configuration, the control inputs are control plane deflections. By contrast, the Fully Actuated Configuration can make use of control plane deflections or the through-body thrusters to control the vehicle.

A. Stability

Stability is a major concern for an AUV. We characterize an unstable vehicle as one that tends to follow an increasingly tightening spiral, from which it cannot recover. This can occur if the destabilizing moment generated by the hull normal force exceeds the stabilizing moment generated by the control planes.

In our simulation, we test for stability by setting an initial velocity and sideslip angle, with zero control plane deflections. Due to the sideslip angle, hydrodynamic forces are generated and the vehicle will begin to turn. A stable vehicle will return to a straight path, reducing the sideslip angle to zero. For an unstable vehicle, the sideslip angle will increase and the vehicle will enter a very tight spiral.

The sideslip angle at which this instability occurs for the C-SCOUT Baseline Configuration varies from 31˚ at 0.5 m/s to 26˚ at 4 m/s. With the Fully Actuated Configuration, the forward control planes further destabilize the vehicle, as they lie forward of the center of mass. As a result the instability occurs at lower sideslip angles of about 22˚, irrespective of vehicle speed. Note that in all these cases, the control planes are not deflected. In practice, use of control planes might allow stable motion at larger sideslip angles.

B. Turning Diameter

In order to determine the turning diameter that each configuration is capable of achieving, based on control planes deflections, we design a test matrix for velocities from 0.5 m/s to 4.0 m/s in 0.5 m/s increments and vertical control plane deflections from 2.5˚ to 15.0˚ in 2.5˚ increments. Due to space constraints, we will present the results for a velocity of 2.0 m/s only.

For the Baseline Configuration, the turning diameter does not change considerably with increasing forward velocity. As expected, the turning diameter of the vehicle decreases with increasing control plane deflection (see *Figure 12*). The vehicle becomes unstable from 0.5 m/s to 4.0 m/s at a control plane deflection angle of 15˚. This is due to the fact that once the vehicle enters the turn, the angle of attack on the vertical control planes increases, possibly exceeding the stall angle, thus reducing the stabilizing moment generated by the control planes (see *Figure 13*).

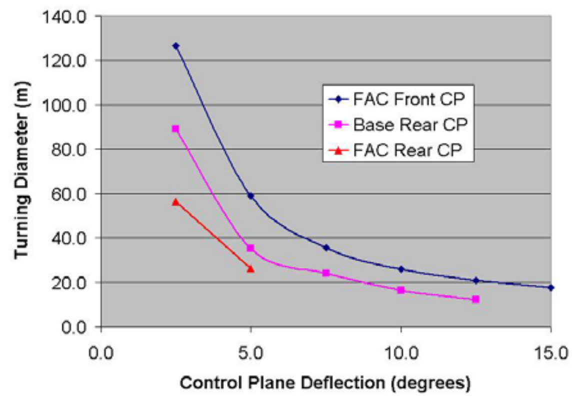

Figure 12 – Turning Diameters for C-SCOUT Baseline and Fully Actuated Configurations at V = 2.0 m/s

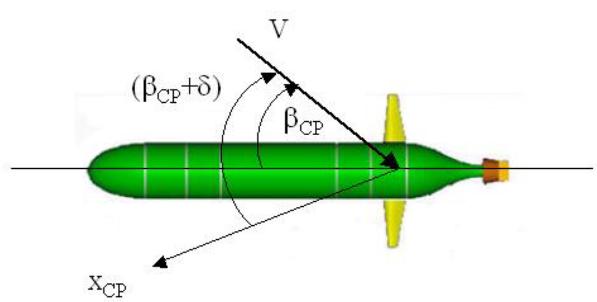

Figure 13 – Angle of Attack Increase on the Rear Control Planes in a Turn to the Right (Top View)

For the Fully Actuated Configuration, a rear control plane deflection of 7.5˚ or more causes the vehicle to enter an unstable spiral. We also note that the smallest turn possible while remaining stable, using the rear control planes, is around 26 m, compared to about 12 m for the Baseline Configuration (see *Figure 12*). If we instead use the forward control planes to turn the vehicle, we find it is more stable. This difference in stability between using the front or rear control planes is due to the direction in which the planes are deflected to turn the vehicle. When we use the rear control planes to turn, the control planes point *away* from the direction of the turn (see *Figure 13*), and the deflection angle is *added* to the sideslip angle to obtain the plane's angle of attack. However, when we use the forward control planes to turn the vehicle, the control planes point *into* the turn (as control planes are forward of the center of mass of the vehicle). In this case, the deflection angle is *subtracted* from the sideslip angle to form the angle of attack on the control planes. This reduces the angle of attack and hence the destabilizing moment. Additionally, the rear control planes are better able to stabilize the vehicle in this maneuver, as they will not stall unless the sideslip angle exceeds the stall angle. Thus we can achieve a turning diameter of 17.5 m with a deflection of 15˚ of the forward control planes (see *Figure 12*).

The use of through-body thrusters in the Fully-Actuated Configuration was examined at forward velocities from 0.1 m/s to 0.5 m/s in 0.1 m/s increments for thruster speeds of 200 RPM to 1000 RPM. The results showed that the use of the thrusters for much of this range reduced the vehicle's stability, especially at lower speeds. Also, the use of the rear thrusters in this range caused the vehicle to be more unstable than when the front thrusters were used. This difference is most likely caused by the asymmetry of the front and rear geometry of the vehicle.

An illustration of the effect of forward velocity and thruster speed on the turning diameter is shown in Figures 14 and 15, respectively. When using the through-body thrusters for turning the vehicle, we observe that, as the forward velocity increases, the turning diameter becomes quite large for low thruster speeds (see Figure 14). Increasing the thruster speed has the effect of significantly reducing the turning diameter (see Figure 15). However using high thruster speeds at low velocities can cause the vehicle to become unstable. Comparing the through-body thruster turning diameter to the control plane turning diameter at a forward velocity of 0.5 m/s, we see that, at high thruster speeds, the through-body thrusters have the capability to turn the vehicle more sharply than the control planes (13.2 m vs 18.5 m using the front planes).

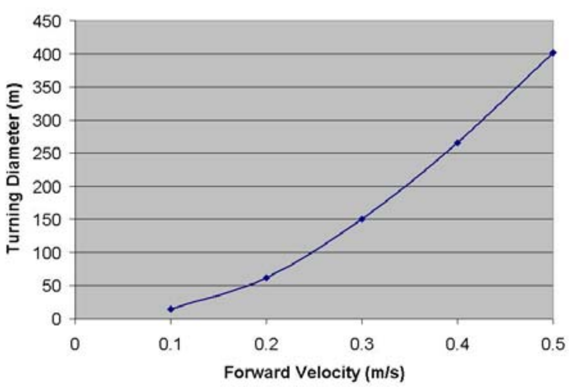

Figure 14 – Turning Diameter for Fully Actuated Config. with Front Through-Body Thrusters at 200 RPM

5. Mission Simulation

C-SCOUT was designed to have the ability to conduct oceanographic sampling missions. We wish to compare the ability of the Baseline and Fully Actuated Configurations of C-SCOUT to successfully complete such a mission.

Typically oceanographic sampling missions are conducted in a 'mower' pattern, consisting of a series of straight tracks, which combine to form a rectangular sampling area. We will define a volume of 100 m by 100 m by 20 m depth in which we would like to sample. Specific points to sample inside this volume consist of 18 waypoints (see *Figure 16*), starting from an initial position of (0,0,0). We adjust the depth of the waypoints along the tracks to illustrate the vehicle's ability to follow a more complex path than simply a planar survey. An example of where this may be useful is if the vehicle needs to follow the contours of the ocean floor.

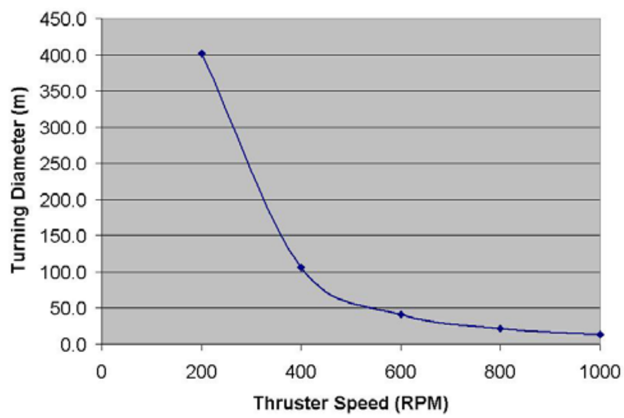

Figure 15 – Turning Diameter for Fully Actuated Config. with Front Through-Body Thrusters at V = 0.5 m/s

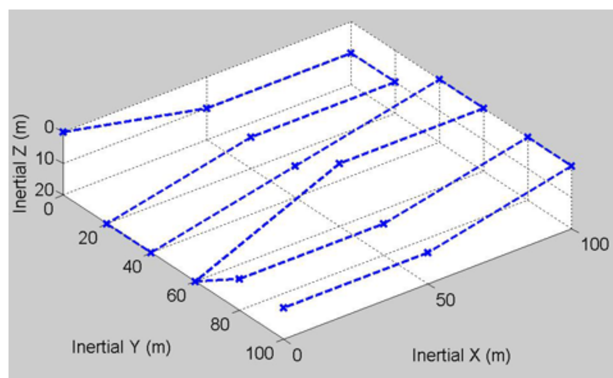

Figure 16 – Mission Sampling Volume and Waypoints

We will define two missions to be evaluated based on these waypoints: one where the vehicle traverses the waypoints without slowing down (continuous sampling), and another where the vehicle must stop at each waypoint to gather data (discrete sampling). We determine that the vehicle has reached a waypoint when it has come within some distance tolerance of that waypoint, which we will set as 2 m. For the Discrete Sampling mission, we will set a sampling time in which the vehicle must remain stationary at the waypoint of 20 s. A situation can occur where the vehicle misses the waypoint on the first pass, and, based on the control system, attempts to loop around to reach the waypoint again. It is possible that the vehicle will continue looping around and never reach the waypoint; therefore we will limit the number of turns to 1.5 turns, or a heading angle change of 540˚, before skipping the waypoint and targeting the next waypoint.

A. Controllers and Control Strategies

In order to give our vehicle simulation autonomous abilities for these missions, we must create a controller and a control strategy for the vehicle.

We define a mission path, which we would like the vehicle to follow, as being a straight line between the waypoints shown in *Figure 16*. We wish to follow this path as closely as possible. We therefore design a controller, which we will call a 'cross-track' controller, which attempts to minimize the distance between the vehicle and the desired path.

We start by defining a new co-ordinate system, with its x-axis pointing from the previous waypoint to the current waypoint that we wish to reach. We can transform the vehicle's coordinates in the inertial frame (designated with the subscript, *I*) to the coordinates in the new frame (designated by the subscript, *CT*) with the following homogeneous transformation matrix:

$$\begin{bmatrix} x_{CT} \\ y_{CT} \\ z_{CT} \\ 1 \end{bmatrix} = \mathbf{T}_{\mathrm{R}} \cdot \begin{bmatrix} X_I \\ Y_I \\ Z_I \\ 1 \end{bmatrix} \tag{34}$$

where the transformation matrix, $\mathbf{T}_{\mathrm{R}}$, is calculated as:

$$\mathbf{T}_{\mathrm{R}} = \mathbf{R}_{\mathrm{y'}} \cdot \mathbf{R}_{\mathrm{Z}} \cdot \mathbf{T}_3 \qquad 35)$$

and $\mathbf{R}_{\mathrm{y'}}$, $\mathbf{R}_{\mathrm{Z}}$,, and $\mathbf{T}_3$ are defined as:

$$\mathbf{R}_{\mathrm{Z}}\left(\psi_{\mathrm{way}}\right) = \begin{bmatrix} c\psi_{way} & s\psi_{way} & 0 & 0 \\ -s\psi_{way} & c\psi_{way} & 0 & 0 \\ 0 & 0 & 1 & 0 \\ 0 & 0 & 0 & 1 \end{bmatrix} \tag{36}$$

$$\mathbf{R}_{\mathrm{y'}}\left(\theta_{\mathrm{way}}\right) = \begin{bmatrix} c\theta_{way} & 0 & -s\theta_{way} & 0 \\ 0 & 1 & 0 & 0 \\ s\theta_{way} & 0 & c\theta_{way} & 0 \\ 0 & 0 & 0 & 1 \end{bmatrix} \tag{37}$$

$$\mathbf{T}_3 = \begin{bmatrix} 1 & 0 & 0 & -X_{prv} \\ 0 & 1 & 0 & -Y_{prv} \\ 0 & 0 & 1 & -Z_{prv} \\ 0 & 0 & 0 & 1 \end{bmatrix} \tag{38}$$

and angles, θ_{way} and ψ_{way} are defined as:

$$\psi_{way} = \tan^{-1}\left(\frac{\left(Y_{nxt} - Y_{prv}\right)}{\left(X_{nxt} - X_{prv}\right)}\right) \tag{39}$$

$$\theta_{way} = -\tan^{-1}\left(\frac{\left(Z_{nxt} - Z_{prv}\right)}{\sqrt{\left(X_{nxt} - X_{prv}\right)^2 + \left(Y_{nxt} - Y_{prv}\right)^2}}\right) \tag{40}$$

where the subscripts, *prv* and *nxt* designate the previous and next waypoints, respectively, and X_i, Y_i, and Z_i are the coordinates of waypoint *i* in the inertial frame.

The cross-track controller directs the vehicle to a target point. This target point lies along the straight line between the waypoints, a distance Δ = 10 m ahead of the vehicle. The target position in the inertial frame can then be calculated as follows:

$$\begin{bmatrix} X_{tar} \\ Y_{tar} \\ Z_{tar} \\ 1 \end{bmatrix} = \mathbf{T}_{\mathrm{R}}^{-1} \cdot \begin{bmatrix} x_{CT} + \Delta \\ 0 \\ 0 \\ 1 \end{bmatrix} \tag{41}$$

Once the target point has been determined, we can use a proportional controller to adjust the control planes to direct the vehicle towards it. Additionally we wish to actively control the vehicle's roll angle, maintaining it as close as possible to zero. We will limit the control plane deflections to ±10° for all four of the control planes. For the Baseline Configuration, the control plane deflections are as follows:

$$\begin{aligned} \left(\delta_{rear}\right)_{top} &= K_p \Delta\psi - K_a \phi \\ \left(\delta_{rear}\right)_{bot} &= K_p \Delta\psi + K_a \phi \\ \left(\delta_{rear}\right)_{prt} &= K_p \Delta\theta - K_a \phi \\ \left(\delta_{rear}\right)_{stb} &= K_p \Delta\theta + K_a \phi \end{aligned} \tag{42}$$

where δ is the deflection of the appropriate control plane, the subscripts *for*, *rear*, *top*, *bot*, *prt*, and *stb* designate the forward, rear, upper, lower, port, and starboard control planes, respectively, K_p and K_a are the heading and roll gains, respectively, and $\Delta\psi$ and $\Delta\theta$ are the horizontal angle error and the vertical angle error, respectively, which are calculated as:

$$\Delta\psi = -\tan^{-1}\left(\frac{Y_{tar} - Y_I}{X_{tar} - X_I}\right) + \psi \tag{43}$$

$$\Delta\theta = \tan^{-1}\left(\frac{Z_{tar} - Z_I}{\sqrt{\left(X_{tar} - X_I\right)^2 + \left(Y_{tar} - Y_I\right)^2}}\right) + \theta \tag{44}$$

For the Fully Actuated Configuration, we have an additional control plane module forward of the center of mass. In Section 4, we found that turning the vehicle using the forward control planes made for a more stable vehicle. Therefore, we choose to use the forward vertical control planes for yaw control. We will use the rear horizontal control planes for depth control, as rapid changes in depth are not required, and therefore an unstable situation is unlikely to occur. We will use all four rear control planes for roll control. In our simulations the forward horizontal control planes are not active, but they could be used for pitch control, as a large pitch angle could be undesirable. We will limit the rear control planes to ±10°, as was done on the Baseline Configuration, and the front control planes to ±15°, as a higher control plane deflection is required to obtain the same turning diameter as the Baseline Configuration. The control plane deflections for the Fully Actuated Configuration are described as follows:

$$\begin{aligned}
\left(\delta_{for}\right)_{top} &= -K_p \Delta\psi \\
\left(\delta_{for}\right)_{bot} &= -K_p \Delta\psi \\
\left(\delta_{for}\right)_{prt} &= 0 \\
\left(\delta_{for}\right)_{stb} &= 0 \\
\left(\delta_{rear}\right)_{top} &= -K_a \phi \\
\left(\delta_{rear}\right)_{bot} &= K_a \phi \\
\left(\delta_{rear}\right)_{prt} &= K_p \Delta\theta - K_a \phi \\
\left(\delta_{rear}\right)_{stb} &= K_p \Delta\theta + K_a \phi
\end{aligned} \tag{45}$$

For the Continuous Sampling mission, rear thruster control is achieved with (33) and control plane deflections are determined by (42) or (45), depending on the vehicle configuration.

For the Discrete Sampling mission we also need to control the speed of the vehicle in order to stop at each waypoint. To accomplish this we define a set of tactics for the vehicle to follow:

- Transit – Traverse the distance between waypoints.
- Approach – Slow the vehicle to a stop at the waypoint.
- Capture – Remain stationary at the waypoint for a set period of time.
- Reorient – (Fully Actuated Configuration only) Use through-body thrusters to reorient the vehicle towards the next waypoint.

The tactics, 'Transit' and 'Approach' both use the control plane deflections listed in (42) and (45) for the Baseline and Fully Actuated Configurations, respectively. For 'Transit', the thrust from the rear thruster is maintained at the value determined by (33). For 'Approach', the thrust from the rear thruster is determined by the following relationship, which will cause the vehicle to slow to a stop at the next waypoint:

$$T = -K_{Tu} u + K_{Tx} d_{wp} \tag{46}$$

where K_{Tu} and K_{Tx} are velocity and distance gains, respectively, and d_{wp} is the distance to the next waypoint.

The tactic, 'Capture' is initiated when the vehicle is deemed to have reached the waypoint. At this point the vehicle has stopped, and the control plane deflections are set to zero. The rear thruster and, if available, the through-body thrusters are used to maintain a stationary position. At this point the vehicle would begin sampling the surrounding water. Once the sampling time has expired, the vehicle will attempt to reach the next waypoint. For the Baseline Configuration, the vehicle returns to the 'Transit' tactic. For the Fully Actuated Configuration, the vehicle initiates the 'Reorient' tactic and uses the through-body thrusters to orient the vehicle towards the next waypoint. Once the vehicle is directed at the waypoint, the 'Transit' tactic is initiated.

B. Mission Evaluation

For the Continuous Sampling mission, the Baseline Configuration does a good job of reaching each waypoint (see *Figure 17*) – only one waypoint is not reached at first attempt. However, that waypoint is reached after looping around. At an equilibrium velocity of 2.0 m/s, the Baseline Configuration completes the Continuous sampling mission in 421.0 s.

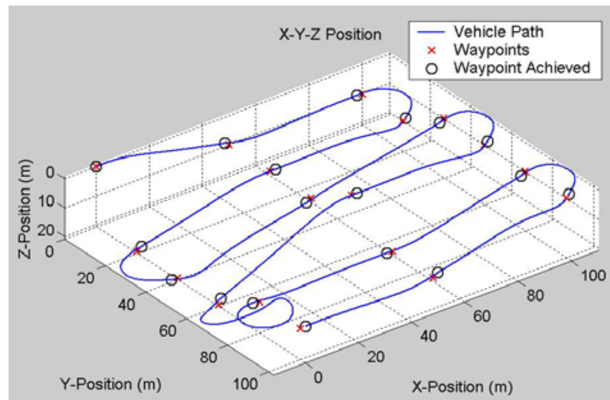

Figure 17 – C-SCOUT Baseline Configuration: Continuous Sampling Mission, Inertial X-Y-Z Plot

The Fully Actuated Configuration has more difficulty than the Baseline Configuration in following the Continuous Sampling mission (see *Figure 18*). We observe vehicle instabilities as it attempts to make a sharp turn, causing the vehicle to turn more quickly than desired and miss the waypoint. The vehicle is able to recover, but is then unable to reach the waypoint. At an equilibrium velocity of 2.0 m/s, the Fully Actuated Configuration partially completes the Continuous Sampling mission, reaching only 13 out of 18 waypoints, in 724.9 s.

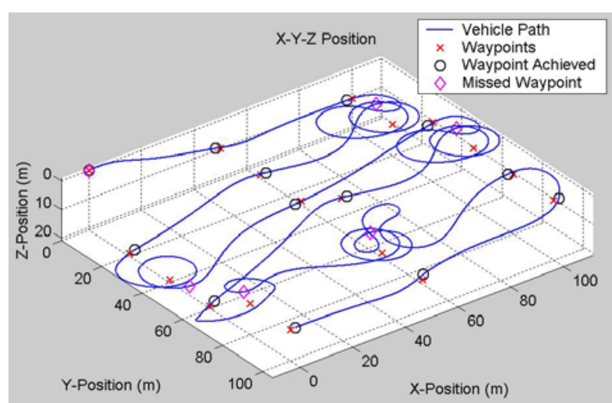

Figure 18 – C-SCOUT Fully Actuated Configuration: Continuous Sampling Mission, Inertial X-Y-Z Plot

For the Discrete Sampling mission, the vehicle stops at each waypoint and remains stationary for the duration of the set sampling time, which we have chosen to be 20 s. For this mission, the Baseline Configuration exhibits some unstable characteristics when the vehicle attempts to make a 90˚ turn from a zero velocity (see *Figure 19*). Additionally, some problems arise after the 12th waypoint, likely due to an error in the control system. At an equilibrium velocity of 2.0 m/s, the Baseline Configuration partially completes the Discrete Sampling mission, reaching 14 out of 18 waypoints, in 1430.9 s.

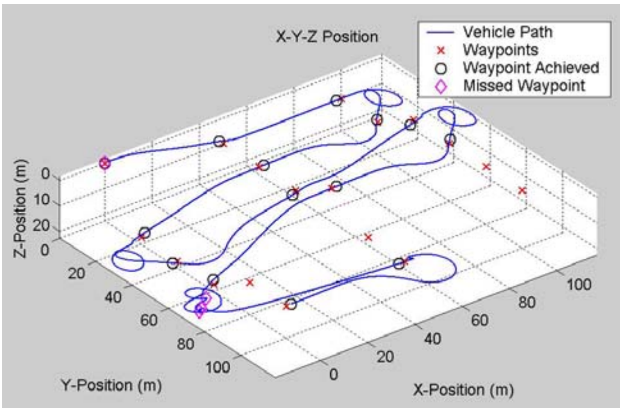

Figure 19 – C-SCOUT Baseline Configuration: Discrete Sampling Mission, Inertial X-Y-Z Plot

The Fully Actuated Configuration performs much better in the Discrete Sampling mission than the Baseline Configuration. The use of the through-body thrusters enables the vehicle to orient itself directly towards the next waypoint, and hence has little difficulty reaching it (see *Figure 20*). At an equilibrium velocity of 2.0 m/s, the Fully Actuated Configuration partially completes the Discrete Sampling mission, reaching 17 out of 18 waypoints, in 1587.2 s.

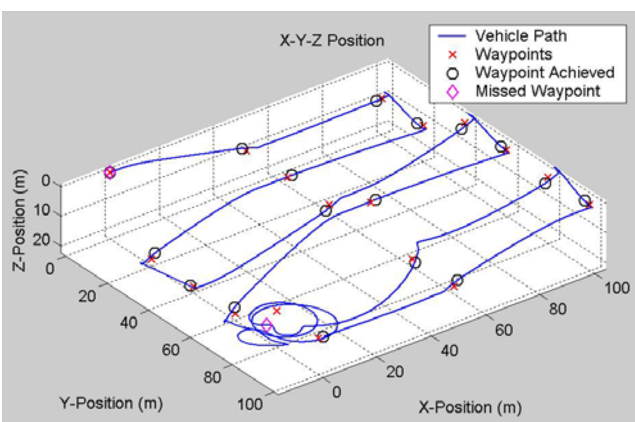

Figure 20 – C-SCOUT Fully Actuated Configuration: Discrete Sampling Mission, Inertial X-Y-Z Plot

6. Conclusions

A dynamics model of a streamlined underwater vehicle has been formulated. The model is capable of the full 360˚ angle of attack range in the calculation of the hull and control plane forces. The vehicle model was validated using field data of ARCS vehicle turning diameters.

The Baseline and Fully Actuated Configurations of the C-SCOUT vehicle are simulated to compare the predicted performance of the two configurations. The Baseline Configuration remains stable except at large control plane deflections. Thus, limiting those deflections can improve the vehicle stability. For the Fully Actuated Configuration, using the front control planes to turn the vehicle can improve vehicle stability. The through-body thrusters in the Fully Actuated Configuration reduce vehicle stability if the vehicle is in motion, especially if high thruster speeds are used at low forward velocities. In all cases, it is expected that the vehicle stability would be further enhanced by improved controllers.

Two simulated oceanographic sampling missions and a set of controllers and control tactics are created to determine circumstances where one configuration of C-SCOUT would be beneficial over the other. We find that the Baseline Configuration is suitable to missions where the vehicle maintains a forward speed. The Fully Actuated Configuration is found to be suitable to missions where it can use its through-body thrusters to change direction once it has stopped. Although it was not studies in this paper, it is expected that the Fully Actuated Configuration would show superior performance in the presence of cross-currents.

References

[1] Marco, D., Healey, A., *Current Developments in Underwater Vehicle Control and Navigation: The NPS ARIES AUV*, Oceans 2000, 2000, Vol. 2, pp. 1011-1016.

[2] Whitney, J., Smith, S., *Observations on the Dynamic Performance of Tunnel Thrusters*, Oceans '98, 1998, Vol. 2, pp. 676-681.

[3] Wang, H., Marks, R., McLain, T., Fleischer, S., Miles, D., Sapilewski, G.,Rock, S., *Otter: A Testbed Submersible for Robotics Research*, Proceedings of ANS 95, 1995.

[4] Mailfert, G., LeMaire, J., *REDERMOR: an Experimental platform for ROV/AUV Field Sea Trials*, Oceans '98, 1998, Vol. 1, pp. 357-362.

[5] Curtis, T., Perrault, D., Williams, C., Bose, N., *C-SCOUT: A General-Purpose AUV for Systems Research*, Underwater Technology 2000, 2000, pp. 73-77.

[6] Pennel, V., Williams, C. D., Bose, N., Veitch, B., Hawbolt, K., Curtis, T., L., Perrault, D., E., O'Young, S., Mukhtasor, Sadiq, R., Husain, T., Ferguson, J., Eaton, G., Reedeker, P., *Innovative Approaches to Environmental Effects Monitoring Using an Autonomous Underwater Vehicle*,

International Workshop on Underwater Robotics for Sea Exploitation and Environmental Monitoring, Rio de Janeiro, Brazil, October, 2001.

[7] Finck, R., *USAF Stability and Control DATCOM*, McDonald Douglas Corp., Global Engineering Documents, 1978.

[8] Hopkin, D., den Hertog, V., *The Hydrodynamic Testing and Simulation of an Autonomous Underwater Vehicle*, Proceedings of the Second Canadian Marine Dynamics Conference, pp. 274-281.

[9] Encarnacao, P., Pascoal, A., *3D Path Following for Autonomous Underwater Vehicle*, Proceedings of the 39th IEEE Conferenceon Decision and Control, Dec. 2000, Vol. 3, pp. 2977-2982.

[10] Cristi, R., Papoulias, F., A., Healey, A., J., *Adaptive Sliding Mode Control of Autonomous Underwater Vehicles in the Dive Plane*, IEEE Journal of Oceanic Engineering, 1990, Vol. 15, No. 3, pp. 152-160.

[11] Humphreys, D., E., Smith, N., S., *Hydrodynamics and Control of a Streamlined UUV Operating at 180-Degree Angle of Attack*, 7th International Symposium on Unmanned Untethered Submersible Technology, 1991, pp. 171-190.

[12] Nahon, M., *A Simplified Dynamics Model for Autonomous Underwater Vehicles*, Autonomous Underwater *Vehicle* Technology AUV '96, 1996, pp. 373-379.

[13] Perrault, D., *Autonomous Underwater Vehicles (AUV) Sensitivity of Motion Response to Geometric and Hydrodynamic Parameters and AUV Behaviors with Control Plane Faults*, Doctoral Thesis, Memorial University of Newfoundland, St. John's, Newfoundland, Canada, 2002.

[14] Prestero, T., *Development of a Six-Degree of Freedom Simulation Model for the REMUS Autonomous Underwater Vehicle*, OCEANS, 2001, Vol. 1, pp. 450-455.

[15] Munk, M., *The Aerodynamic Forces on Airship Hulls*, Report No. 184, National Advisory Committee on Aeronautics (NACA), 1924.

[16] Allen, H., Perkins, E., *Characteristics of Flow Over Inclined Bodies of Revolution,* Research Memorandum RM A50L07, National Advisory Committee on Aeronautics (NACA), 1951.

[17] Hopkins, E., *A Semiempirical Method for Calculating the Pitching Moment of Bodies of Revolution at Low Mach Numbers*, Research Memorandum RM A51C14, National Advisory Committee on Aeronautics (NACA), 1951.

[18] Jorgensen, L., *Prediction of Static Aerodynamic Characteristic for Space-Shuttle-Like and Other Bodies at Angles of Attack from 0˚ to 180˚,* NASA TN D-6996, January 1973.

[19] R. Thomas*, Performance Evaluation of the Propulsion System of the Autonomous Underwater Vehicle C-SCOUT*, Master's Thesis (in preparation), Memorial University of Newfoundland, St. John's, Newfoundland, Canada, 2003

[20] Abbott, I. H., Von Doenhoff, A. E., *Theory of Wing Sections*, Dover Publications, 1959.

[21] Reigels, F. W., *Aerodynamische Profile*, Muchen, R. Oldenbourg, 1958.

[22] Critzos, C. C., Heyson, H. H., Boswinkle Jr., R. W., *Aerodynamic Characteristics of NACA 0012 Airfoil Section at Angles of Attack From 0º to 180º*, NACA TN 3361, 1955.

[23] McCormick, B. W., Aerodynamics, Aeronautics, and Flight Mechanics, New York, Wiley, 1995.

[24] Saunders, A., *The Effect of Velocity and Orientation on the Simulation and Experimental Characterization of an AUV Tunnel Thruster*, Masters Thesis, University of Victoria, Victoria, British Columbia, Canada, 2003.

[25] Ferguson, J. and Jackson, E., *Design of ARCS-Autonomous Remotely Controlled Submersible*, ROV 1984 Conference Proceedings, Apr 1984, pp 365-368.